RSC Advances

RSC Publishing

PAPER

View Article Online
View Journal | View Issue

Cite this: *RSC Advances*, 2013, **3**, 7296

High performance cascaded PDMS micromixer based on split-and-recombination flows for lab-on-a-chip applications†

Hamid SadAbadi, Muthukumaran Packirisamy* and Rolf Wüthrich

Received 24th January 2013,
Accepted 22nd February 2013

DOI: 10.1039/c3ra40910d

www.rsc.org/advances

In this paper a cost-effective and simple 3-layer PDMS passive micromixer has been designed, optimized, simulated, fabricated and successfully characterized. The mixing mechanism is based on splitting and recombining the flow. The designed micromixer was simulated and a method was formulated to assess the mixing performance. The mixer has shown excellent mixing efficiency over a wide range of flow rates specifically at low flow rates. The experimental measurements were performed to qualify the mixing performance of the realized mixer. The results show that predicted mixing efficiency is comparable with experimental results. A high mixing efficiency of 85% was obtained at flow rates below 40 μL min^{-1} meaning the possibility of obtaining full mixing for Reynolds number R_e <5.5. Due to the simple channels' configuration of the device, the simulations show that its pressure drop is less than 1 kPa at flow rate of 50 μL min^{-1}. In cases where very high mixing efficiency is demanded, several micromixers (mixing units) can be easily combined to form a cascaded mixing module. The results show even with a combination of two units, an efficiency as high as 80% can be achieved at a high flow rate of 100 μL min^{-1}, which can be considered as full mixing. One of the main advantages of the device explored in this work is its small dimensions (1.5 × 2.3 mm) which makes it possible to be easily integrated with PDMS based microfluidic devices for different point-of-care applications.

1. Introduction

While the microfluidic technology has been maturing well, a big surprise is that LoC systems are still not being used extensively. Through the fabrication of microfluidic devices which possess two fundamental and demanding features including "*low-cost*" and "*simple*", it is very likely to move toward the next step of using LoCs for wide applications.[1]

One of the most challenging tasks in the LoC systems is efficient mixing. In biochemical analysis systems which work under microfluidic environments, achieving of better mixing in a short period of time as well as a short fluidic system is crucial in order to improve the reaction. Due to low Reynolds number in microfluidic systems (flows with $R_e \approx 0.01$–10), the flow regime is laminar and consequently the mixing mechanism becomes mostly diffusion dominant.[2–4]

Micromixers are generally classified into two main categories: passive and active. In passive micromixers, the mixing is performed by changing the geometry of the mixer in order to alter the flow direction to induce disturbances such as recirculations that create the transversal mass transport. In contrast, active micromixers rely on an external energy source for mixing.[4–7] Compared to active mixing mechanisms, passive micromixers can have simpler design and therefore can be well integrated for lab-on-a-chip (LoC) application.[8,9]

Besides being low-cost and simple, another important issue that has to be considered in the design of micromixers is their working flow rate which strongly depends on their applications. Micromixers are mostly used in two main categories including chemical microreactors and in immunoassay biosensors.[10] Microreactors that are used for synthesis applications, operate normally at relatively small flow rates.[11–13] For an example, in organic synthesis, reduced flow rates (corresponding to larger residence times) is highly demanded to be able to synthesize detectable products.[14] Moreover, in biosensing applications, the flow rate should be small enough to enhance biomolecule interactions in order to achieve an acceptable sensitivity.[15] Typical flow rates for these applications are 1–20 μL min^{-1} or less[12,15–18] indicating that the mixing is determined mostly by diffusion.

In the last decade, various types of passive micromixers have been developed and fabricated including 2D structures such as tesla structure,[9] sawtooth structure,[19] and various T-type mixing mechanisms with obstacles[20] and fin arrangements[21] inside the microchannels. Through these structures,

Optical Bio-Micro Systems Laboratory, Mechanical and Industrial Engineering, Concordia University, EV 4.139 1455 de Maisonneuve Blvd. West, Montreal, Quebec, Canada, H3G 1M8. E-mail: pmuthu@alcor.concordia.ca

† Electronic supplementary information (ESI) available. See DOI: 10.1039/c3ra40910d

researchers try to increase the possibility of creating disturbances for better performance.[22] However, their acceptable performance could only be achieved in high flow rates ($\sim$100 μL min^{-1} and more) which are too far from the applicable range mentioned earlier.[2,9,20,23,24] Furthermore, another drawback of these micromixers is the long length of the microchannels, which are in the order of a few centimeters.[9,25]

Several complex 3D structures have been proposed in order to achieve higher efficiency in shorter lengths.[26,27] Examples include 3D structures for twisting flow[3] and *split-and-recombine* structures.[23,25,26,28,29] Nevertheless, they used very complicated 3D structures that use multiple fabrication steps which make them to be far from being "*cheap*" and "*simple*".[25–30] Using polymeric materials for low-cost fabrication of micromixers is a good example of enabling wide applications of integrated LoC devices.[24,28,31]

In the present paper, we propose a 3D micromixer with high efficiency, based on split-and-recombination of the flow. We attempt to reach "*cheap*" and "*simple*" goals by introducing a simple 3-layer PDMS structure. The device is designed and optimized. The mixing is simulated and its performance is compared to that of a *T*-type mixer by developing a new mathematical-based method for the estimation of the mixing efficiency. The micromixer was fabricated and the flow is visualized in the chip. Finally, a mixing experiment was accomplished to evaluate its performance quantitatively in the real conditions. The results show a very good mixing performance at low flow rates (1–20 μL min^{-1}). Due to the simplicity of the proposed micromixer, the mixing unit can be easily integrated with micro-total analysis systems (μ-TAS).

2. Design

2.1 Design principle

The proposed passive micromixer is based on the split-and-recombination of flow to maximize the surface contact between two fluids of interest. The mixing mechanism of a T-type mixer and the proposed mixer is shown in Fig. 1. In the Fig. 1a, a T-type mixer is depicted. The T-type streamlines show that there is only one contact area between the two fluids. In this figure, the concentration distribution along the microchannel is also shown.

As shown in Fig. 1b, the proposed device has a microchannel configuration that can guide the fluids to produce alternate layers at the outlet in order to maximize the diffusion. The input fluids 1 and 2 were dispensed equally in a set of microchannels and then were re-arranged in a new layered configuration. In the design, there are two simple T-type sub-micromixers which will be mixed at the final step to have a complete mixing. Through this design, each inlet is dispensed into two sub-streams and at the final stage they will be reunified in a way that maximizes the surface contact between the two flows of interest.

A 3-D view of the device is shown in Fig. 2a. From this figure, it can be seen that, the micromixer contains 3 layers. The fluid 1 in the first (bottom) layer will be dispensed into two sub-streams and will be carried through the second layer into the third (top) layer where mixing will happen with the fluid 2 which is already dispensed in this layer.

2.2 Optimization of the micromixer dimensions

In order to maximize the mixing performance, we should adjust the channel widths W_i where i = 1, 2, 3, 4. The dimensions are schematically shown in Fig. 2a. The maximum performance for a specific inlet flow rate can be reached, when each microchannel with the width of W_i contributes equally to

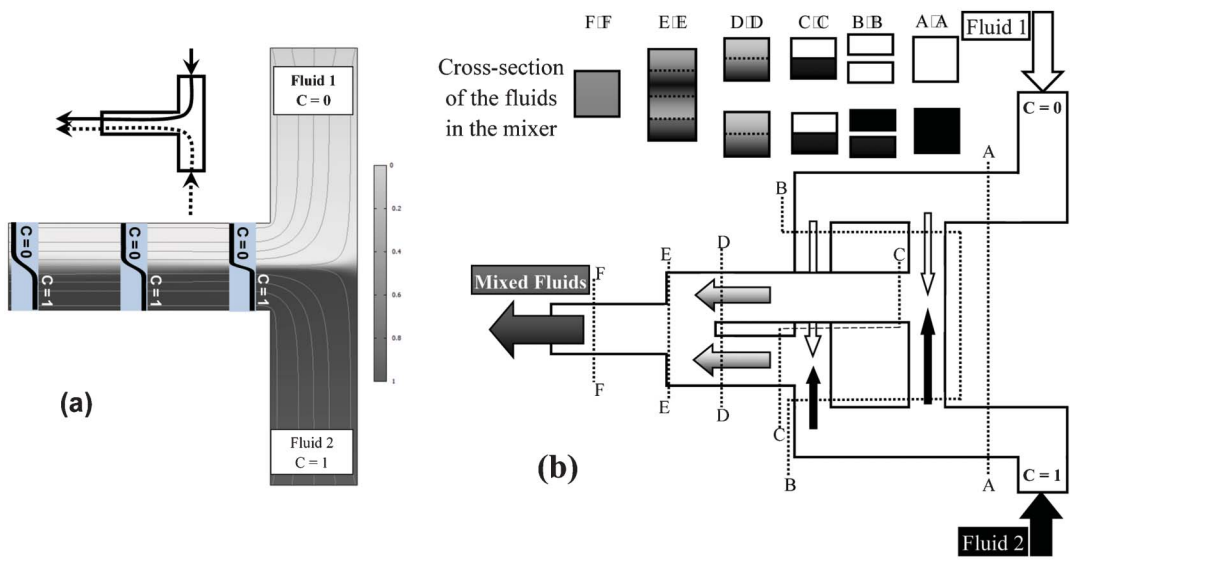

Fig. 1 Mixing mechanism; (a) T-shape mixer; (b) the proposed 3-layer micromixer. Each inlet is split into two sub-streams. The streams are finally recombined at the outlet.

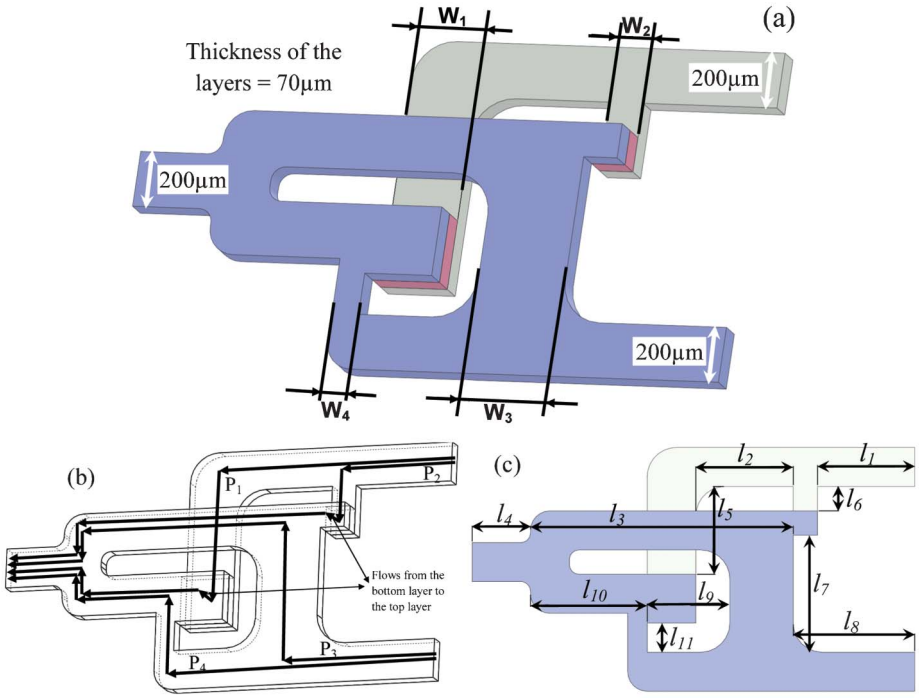

Fig. 2 The 3D view of the micromixer. (a) The variables namely, the width of the channels (W_1–W_4) have to be optimized to have equal contributions from the inlets to maximize the mixing performance, (b) four available paths (p_1 to p_4) from inlets to the outlet, (c) micromixer dimensions used for optimization.

the outlet flow. Darcy–Weisbach equation of *head loss* in channel was used to mathematically express how each part of the inlet (with the size of W_i) undergoes head loss from inlet to the outlet. Head loss (h) in a pipe with the length of L can be obtained from the following equation:[32]

$$h = f\frac{L}{D}\frac{V^2}{2} \quad (1)$$

Where D is the pipe hydraulic diameter and it is equal to $D = 4A/P$, where A and P are area and perimeter of the channel, respectively, V is the fluid velocity and f is the friction factor that is determined experimentally. For low Reynolds number (R_e) flow or laminar flow regime which is applicable in microfluidic systems, there is a simple relation between *Darcy* friction factor, f, and R_e that can be expressed as the following equation:[32]

$$f = \frac{C}{R_e} \quad (2)$$

Where, R_e is Reynolds number and $R_e = \rho VD/\mu$ where ρ is the fluid density and μ is the dynamic viscosity of the fluid and the constant C is tabulated for a different duct shapes. For the rectangular channel with dimensions of 200 μm × 80 μm (aspect ratio of 2.5) the value of C correspond to 64 ($C \approx 64$).[33] In addition to the head loss in the pipe, there are also minor head losses (h_m) in bends, Tees (both combining and dividing), *etc.*, which can be calculated from the equation $h_m = KV^2/2$ where K is the friction coefficient that is determined experimentally and is tabled in the fluidic handbooks.[32]

Considering the thickness of t for the microchannels, when the flow with the rate of Q is flowing in a channel with a width of W and a length of L, the following equation can be used to calculate the head loss:

$$h = \frac{8\mu QL}{\rho}\frac{(t+W)^2}{h^3W^3} \quad (3)$$

There are two possible flow paths from each inlet to the outlet. Hence, we have the total of four possible paths from the inlets to the outlet as shown in Fig. 2b by P_i where i = 1 to 4. The value of head loss in each path is assumed to be h_i where i = 1, 2, 3, 4. Head loss in each path is a function of the variables (W_i) and the length of the channels (l_j where j = 1 to 11) as shown in Fig. 2c. In addition, in each pass, there are bends, Tees or change in the channel dimensions, which produce minor head losses (h_m) and should be considered in the calculation of total head loss in each pass. So the head losses, h_i, in paths P_i are as follows:

$$\begin{aligned} h_1 &= f_1(W_1, W_2, W_3, W_4, l_j) + h_{m_1} \\ h_2 &= f_2(W_1, W_2, W_3, W_4, l_j) + h_{m_2} \\ h_3 &= f_3(W_1, W_2, W_3, W_4, l_j) + h_{m_3} \\ h_4 &= f_4(W_1, W_2, W_3, W_4, l_j) + h_{m_4} \end{aligned} \quad (4)$$

In this design, the length l_j are selected as constant and therefore the head losses are only dependent of variables W_i. In order to have equal flow rates through these paths, head losses, h_i, should be equal as defined by the following conditions that are applied for widths optimization:

$$\begin{cases} h_1 = h_2 \\ h_1 = h_3 \\ h_1 = h_4 \end{cases} \rightarrow \begin{cases} h_1 - h_2 = 0 \\ h_1 - h_3 = 0 \\ h_1 - h_4 = 0 \end{cases} \quad (5)$$

As we can see, there are four unknowns and three equations. In order to be able to solve this set of nonlinear and coupled equations, a constraint is created by setting W_4 = 75 μm while the other three widths (W_1, W_2, and W_3) are determined. The optimum widths are obtained as the following: W_1 = 200 μm, W_2 = 100 μm, W_3 = 260 μm and W_4 = 75 μm.

3. Simulation model

The simulation of the mixer with optimized dimensions is performed to evaluate the mixing performance under different inlet flow rates. The COMSOL® Multiphysics MEMS module is used for the finite element (FE) analysis of the Navier–Stokes incompressible fluid flow in microfluidic environment. The water is used as the fluids to be mixed containing solutes with two different concentrations of C = 0 and C = 1 in order to have normalized concentration at the outlet. The diffusion coefficient of the solute in water was set to 2.5 × 10^{-10} m s^{-2}. FEM of the 3D CAD model is used for simulation. An initial study on the effect of element sizes, show that element sizes less than 4.5 μm will not improve the precision of the results but the CPU time. Therefore, the whole 3D volume is discretized with the maximum element size of 4.5 μm. The convergence limit for the normalized relative error was set 1 × 10^{-7}.

3.1 Simulation performance assessment

As mixing takes place the molar concentration on one inlet of the mixer decreases from 1, while on the other side it increases from 0. Complete mixing is achieved when the concentration of the mixture reached 0.5. Generally, to quantify the simulation results, the cross section image of the outlet is obtained in gray-scale pixel intensity. Then the standard deviation of the pixel intensity distribution of the image is measured to calculate the efficiency.[3,21,25,26] However, in this paper, we established a simpler method based on similar principal in order to quantitatively assess the simulation results. This method is mathematically simpler than the conventional methods as it does not need any image processing. Our calculations confirmed that both methods lead to practically identical results. In this method, first, the profile of concentration in the outlet is obtained along a line at the middle of its depth. In Fig. 3a and Fig. 3b, typical variation of concentration for a T-type and for the new mixer is shown by a black line and is presented by the function $f(x)$, where x is the normalized width. In this figure, the red line indicated as the function $f_1(x)$ corresponds to the worst case when there is no diffusion between the two fluids of interest. The green line, which is denoted by the function $f_2(x)$, depicts the case when the fluids were fully mixed and the value of $f_2(x)$ would be 0.5 in all cases.

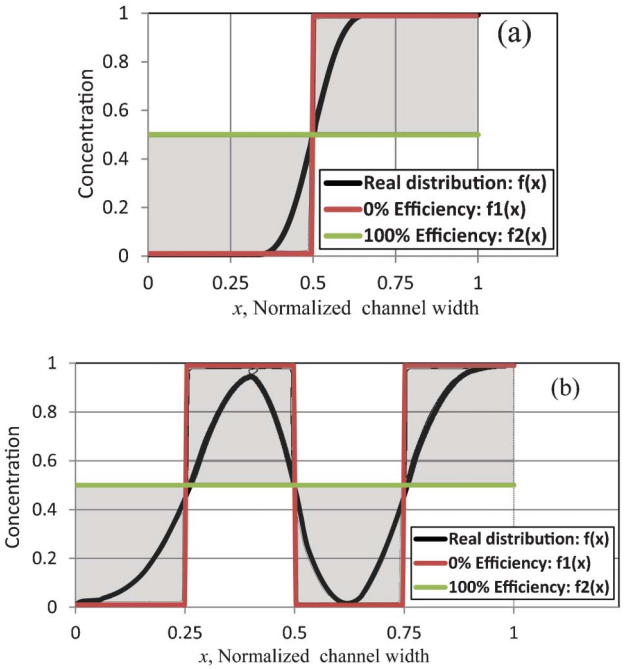

Fig. 3 Performance assessment of mixing; (a) T-type micromixer, (b) proposed micromixer.

The hatched area, which is the difference between $f(x)$ and $f_1(x)$ in Fig. 3, represents the degree of diffusion of one fluid into the other. Mixing efficiency, η, is thus defined as the ratio between the hatched area corresponding to actual mixing, and the area between $f_2(x)$ and $f_1(x)$ corresponding to full mixing, as:

$$\eta = \frac{\textit{area corresponding to actual mixing}}{\textit{area corresponding to full mixing}} = \frac{\int_0^1 |f_1(x) - f(x)|dx}{\int_0^1 |f_2(x) - f_1(x)|dx} = \frac{\int_0^1 |f_1(x) - f(x)|dx}{0.5} \quad (6)$$

The area corresponding to full mixing (shown in gray in Fig. 3a and Fig. 3b) between green and red lines is equal to 0.5 as the final concentration is equal to 0.5 and the width of the channel is normalized. This η will be used for performance characterization.

3.2 Simulation results

The simulation performed by using the mentioned parameter and the results for T-type and the proposed device are depicted in Fig. 4a and Fig. 4b respectively. The results show that the flow rates passing through the channels with the optimized widths of W_1 to W_4, are very close, with less than 1.5% variation, and it proves that the optimization was successful.

In order to compare the efficiency between the proposed and T-type mixers, the variation of concentration is obtained at a distance of 3.8 mm from the inlet that is along the C–C cross-section in Fig. 4a and Fig. 4b and the mixing efficiency, η, was obtained at this section. Even though the actual channel length at the measuring section for the proposed mixer is

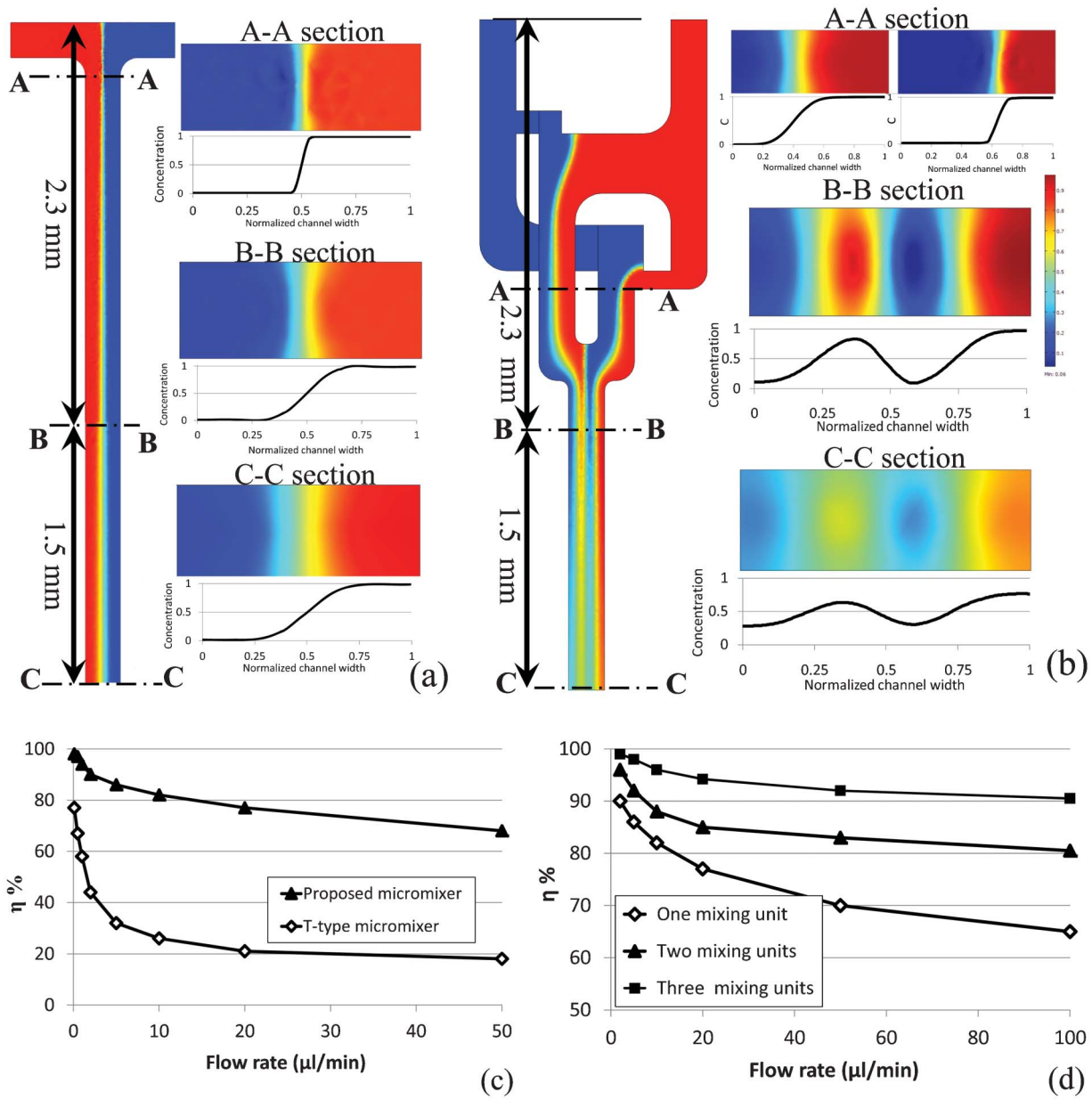

Fig. 4 Simulation results; (a) T-type mixing at a flow rate of 20 μL min^{-1} with η = 20.9%; (b) the proposed micromixer at a flow rate of 20 μL min^{-1} with η = 76.3%; (c) comparison of mixing performance of the proposed mixer and a T-type micromixer at different flow rates; (d) mixing performance with different cascaded combinations of mixer units at different flow rates.

slightly longer than the length of T-mixer by the thickness of the middle layer due to 3D configuration, same chip distance is chosen to obtain minimum footprint. The simulation results for the flow rate of 20 μL min^{-1} are shown in Fig. 4a and Fig. 4b. In these figures, the distribution of concentration at three different cross-sections of the channel is shown for each mixer. In addition, variation of concentration at the middle line is also shown for the proposed and T-type mixers.

Based on the performance criteria, the new mixer can achieve a mixing efficiency as high as 76% even at a high flow rate of 20 μL min^{-1} ($R_e \sim 3$) while a T-type mixer shows only η = 21%. The mixing efficiency for various flow rates between 0.2 μL min^{-1} and 50 μL min^{-1} is shown in Fig. 4c. Considering the mixing efficiencies of higher than 80% for fully mixed flows, the proposed mixer can achieve full mixing for flow rates up to 15 μL min^{-1} (R_e <2.2).

One could note that the increase in diffusional area in the proposed mixer by nearly 3 times compared to a standard T-type mixer. In addition, the diffusional length is also higher for the 3D configuration due to the additional middle layer. Hence, one can expect an increase in the performance by more than 3 times due to the combined effect of increase in diffusional area and length. This is in agreement with the

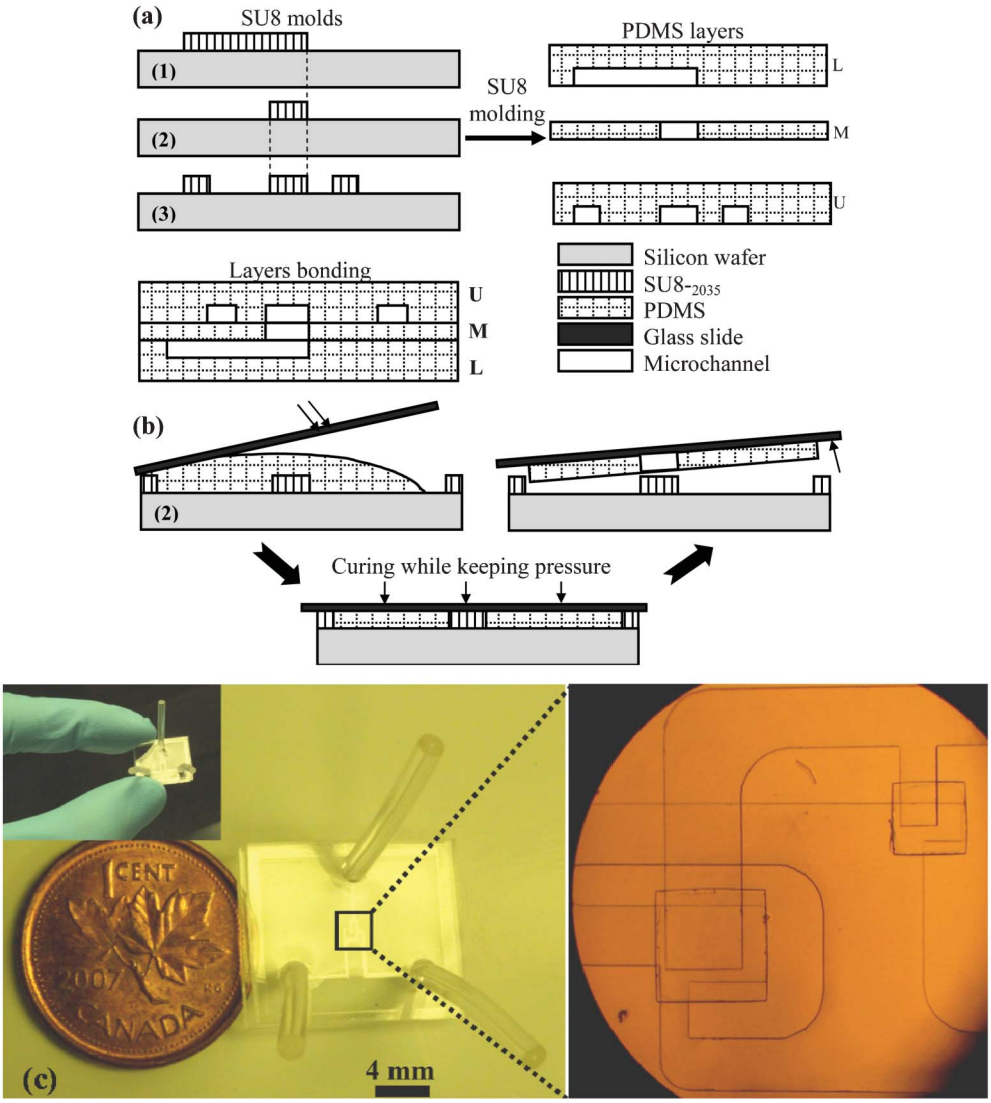

Fig. 5 Fabrication process of the micromixer; (a) three SU8 molds used for fabrication of the mixer; (b) PDMS thin layer fabrication process to make the middle layer (80 μm thick); (c) the fabricated device and the close-up shows how 3-layers are aligned to form the mixer.

estimated mixing efficiency of $\eta_{\text{proposed}} \approx 76\%$ and $\eta_{\text{T-type}} \approx 21\%$ showing a mixing improvement of 3.6 times.

Fig. 4c indicates very high efficiency for the low flow rates due to the enhanced diffusion-based mixing mechanism of the proposed mixer. However, there is a relatively low mixing performance for high Reynolds numbers (R_e >4.0) when the flow rate is higher than 30 μL min^{-1}. There is a promising way to resolve this problem by combining several mixing units. Considering the proposed micromixer as a mixing unit, one can cascade several mixing units to build a mixing module. The mixing performance for two different combinations of the micromixers in cascade for various flow rates between 2 μL min^{-1} and 100 μL min^{-1} is shown in Fig. 4d. More simulation results can be found in the ESI.†

4. Fabrication

The proposed micromixer was fabricated using poly(dimethylsiloxane)(PDMS). Sylgard® 184 elastomer kit from Dow Corning Corporation was used for PDMS fabrication. For fabrication, the base polymer (pre-polymer) and the curing agent (cross-linking agent) are mixed with 10 : 1 ratio by weight. The device consists of three PDMS layers. Therefore, there are three individual masks for the fabrication of the mold for each layer.

The schematic of fabrication steps of the mixer is depicted in Fig. 5a. In this figure, three SU8 molds and their corresponding PDMS layers include lower (L), middle (M) and upper (U) layers are shown. Standard patterning of SU8-2035 photoresist (from MicroChem) was used for the fabrication of the molds. For each layer, the SU8 was spin coated with a thickness of 80 μm (at 500 rpm for 10 s followed by 1500 rpm

for 35 s) and then soft baked at 95 °C for 12 min. The soft backed SU8 then was exposed to UV light followed by a post baking process for 10 min at 95 °C. After that, the SU8 was developed and finally the mold is hard baked at 150 °C for 30 min. To be able to use these layers as a mold for PDMS fabrication, all molds are silanized.

As shown in Fig. 5a, the proposed PDMS device includes two thick layers (U and L) and a thin middle layer (M) with a thickness of 80 μm. The fabrication process of the thin layer (M), is schematically shown in Fig. 5b. For the fabrication of the thin layer, PDMS was poured on the mold and then a semi-silanized glass slide was placed on PDMS to let the excess of PDMS to be removed from the mold. While keeping the pressure on the glass slide, the PDMS thin layer was cured at 100 °C for an hour. Afterwards the semi-silanized glass slide with PDMS thin layer (M), can be easily peeled off from the mold as the mold was already silanized. Oxygen plasma was used to bond the middle layer to the bottom thick PDMS layer. After this bonding, the glass layer is replaced by the top thick PDMS layer to seal the channels. The fabricated device is then used for real mixing experiments and flow visualization.

One of the important issues in the bonding process is the correct alignment of the layers. This is crucial as the middle thin layer allows the fluid to be passed through its hole from the first (bottom) layer to the third (top) layer. Therefore, any miss-alignment will result in malfunctioning of the device. A clearance of 15 μm is considered in the size of features of middle layer in order to reduce the bonding errors due to miss-alignment. These size changes are also considered in the calculation of minor head losses for finding the optimum channel widths.

5. Experimental mixing results

5.1 Flow visualization

In order to characterize the realized device and compare the predicted efficiency with the experimental results, red and green colored water was introduced to the inlets. A syringe pump is used to pump two dies with different flow rates. A camera attached to a microscope recorded the visualized flow. The experimental results for the flow visualization show the efficient mixing of two fluids. Fig. 6 shows the flow of the two colored fluids in the microchannels and demonstrates how the sub-streams split into two flows and then combine into the outlet. In the Fig. 6a a high flow rate of 400 μL min^{-1} was used ($R_e \sim 55$) to diminish diffusion and to show four equal sub-streams in the outlet. These equal sub-streams in the outlet prove that the optimization part was successful. In Fig. 6b, the mixing is shown at a flow rate of 40 μL min^{-1}. Form this figure it can be observed that the thickness of the green flow is diminishing along the flow which shows that the flows are mixing efficiently by diffusion.

5.2 Mixing testing of acid and base

In the previous experiment, the mixing is assessed qualitatively by using the colored liquids. In order to determine the performance of the proposed micromixer quantitatively, an experimental layout is designed to obtain the variation of mixture concentration profile at the outlet. Fig. 7a and Fig. 7d show the layout and the fabricated chip, respectively.

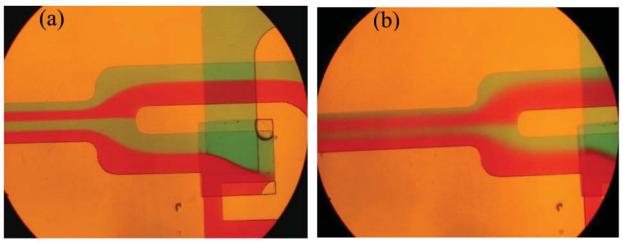

Fig. 6 Flow visualization of the proposed micromixer using green and red flows. (a) High flow rate of 400 μL min^{-1} ($R_e \sim 55$) to minimize the diffusion for better visualization; (b) the thickness of the green flow is decreasing along the flow which shows the green flow is diffusing into the red at rate of 40 μL min^{-1} ($R_e \sim 5.5$).

In order to assess the performance of mixing, variation of pH value along the width of the channel is measured by branching the outlet into four branches as depicted in Fig. 7a. More number of branches would be beneficial for better evaluation of the pH variation in the channel. However, it is not feasible to have more than four branches for a channel of 200 μm width. The outlet of mixer channel is divided into four branches with equal width as a result of having four sub-streams in the micromixer outlet. Indeed, the branching layout was designed in such a way to have equal head-loss in all branches and therefore to have identical flow rates. The pH value which is measured in each branch is considered to represent the average pH at the middle point of each sub-stream as schematically depicted in Fig. 7a.

The mixing experiments were carried out by mixing a strong acid (hydrochloric acid) and a strong base (sodium hydroxide). 0.83 mL of concentrated HCl (37%) from Fisher Scientific was diluted into 1L of DI-water to make 10 mM HCl solution with a pH of 2. Similarly, 400 mg of NaOH was dissolved in 1L DI-water to have a 10 mM base solution with a pH of 12. The solutions were introduced into the mixer with similar flow rates using a syringe pump. Each outlet was collected and a pH-meter was used to measure the pH value. A WTW pH 315i pH-meter with measurement accuracy of ± 0.01 pH was used. The tests were performed at different inlet flow rates.

The efficiency is estimated based on the mixing of equal amounts of acid and base to yield a mixture with a pH of 7. As mixing takes place the pH value of inlet#1 of the mixer increases from 2, while on the other side, the pH value of inlet#2 decreases from 12. Complete mixing is considered when the pH of the mixture reaches to the value of 7. A typical measured pH variation that was used to estimate the efficiency is shown in black in Fig. 7b corresponding to a flow rate of 200 μl min^{-1}. This graph is denoted as the function $p(x)$ where x is the normalized outlet channel's width and changing between 0 and 1. The branch 1 defined by the range ($0 \leqslant x \leqslant 0.25$) in Fig. 7b, is mainly supplied from the inlet#1. Due to the mixing, the pH value of the fluids in this branch increase from 2 to a

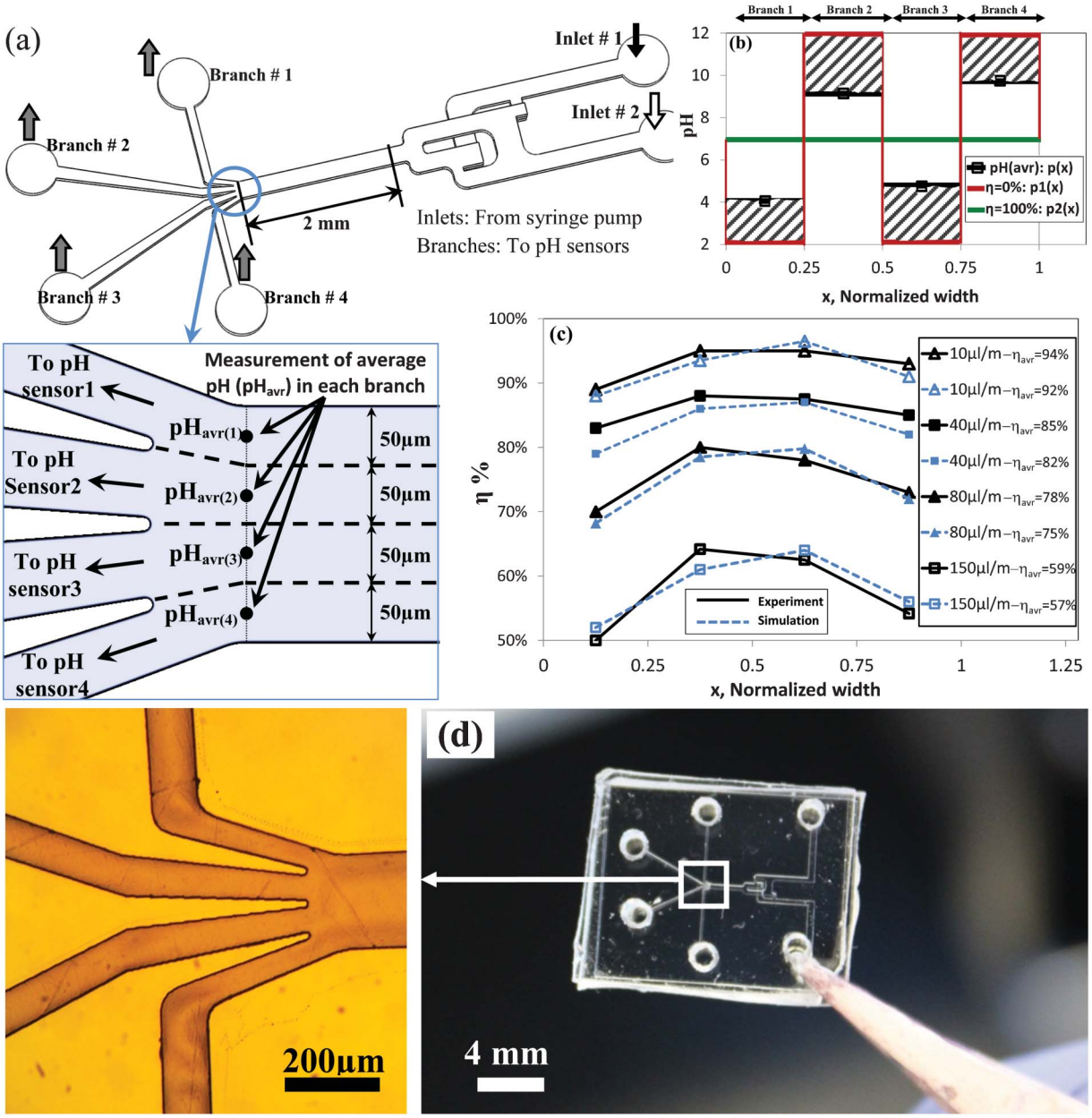

Fig. 7 Evaluation of the micromixer performance in real conditions; (a) a layout with four branches designed to precisely measure the variation of pH in the cross-section of the mixer outlet, (b) measured pH used for estimation of efficiency. The black line shows measured values and the hatched area represents the mixed fluids, (c) the variation of efficiency along the outlet cross-section and the average efficiency for each flow rates for both experimental (solid line) and simulations (dashed line) measurements, (d) the fabricated device.

value of ≈ 4 as shown in Fig. 7b which indicates the degree of mixing, considering the ideal mixing with pH of 7. Similar mixing of acid is happening in 3rd branch ($0.5 \leqslant x \leqslant 0.75$). One could extend this explanation for decrease in pH from 12 for the branch 2 ($0.25 \leqslant x \leqslant 0.5$) and branch 4 ($0.75 \leqslant x \leqslant 1$). Thus, hatched area in Fig. 7b represents the actual mixing. In Fig. 7b red and green lines correspond to no-mixing and full-mixing situations and are denoted by the functions $p_1(x)$ and $p_2(x)$, respectively. Considering equal flow rates from all the branches, the following equation was used to calculate the efficiency in the first branch:

$$\eta_{x=0.125} = \frac{\textit{area corresponding to actual mixing}(0 \leq x \leq 0.25)}{\textit{area corresponding to full mixing}(0 \leq x \leq 0.25)} = \frac{\int_0^{0.25} |p_1(x) - p(x)|dx}{\int_0^{0.25} |p_2(x) - p_1(x)|dx} \quad (7)$$

Similar equation can be used to calculate efficiency in other branches by changing the integral limits. The mixing efficiency in each outlet was obtained and then was plotted against the channel widths at four different points including x

= 0.125, 0.375, 0.625, and 0.875 to obtain the variation of efficiency along the outlet cross-section for each flow rate. Furthermore, to have the average mixing efficiency, the following equation has been used:

$$\eta_{avr} = \frac{area\ corresponding\ to\ actual\ mixing (0 \le x \le 1)}{area\ corresponding\ to\ full\ mixing (0 \le x \le 1)} = \frac{\int_0^1 |p_1(x) - p(x)| dx}{\int_0^1 |p_2(x) - p_1(x)| dx} \quad (8)$$

Detailed discussions of the efficiency calculation can be found in the ESI.†

The variation of efficiency along the outlet cross-section at different flow rates is shown in Fig. 7c. The average efficiency (η_{avr}) for each flow rate is also shown in this figure. From this graph is it clear that the mixer achieves very high efficiencies specifically at low flow rates. The two liquids can be assumed as fully mixed for the flow rates less than around 50 μL min^{-1}.

In order to verify the test results, the tested layout was simulated under different flow conditions. The simulation results show that the flows passing through four branches are almost equal with a maximum variation of 2.3% compared with the ideal condition of equal flow rates. The comparison of predicted and experimental values for mixing efficiency show good agreement as shown in Fig. 7c. There is a maximum of 4.1% difference in efficiency between predicted and experimental results. For example, the value of average efficiency, η_{avr}, for a flow rate of 10 μL min^{-1} is 94% for experimental test and 91.8% from the prediction (simulation) result, which indicates 2.2% difference. For the flow rate of 150 μL min^{-1}, the difference between the experiment and prediction is less than 1.9%. More detailed simulation results can be found in the ESI.†

6. Conclusion

A "*simple*" and "*cheap*" PDMS micromixer is designed, optimized, fabricated, and successfully characterized in this paper. The 3D mixing mechanism is based on *split-and-recombinant* flows through a 3-layer design. The mixer channel dimensions are then optimized in order to reach high performance. A quantitative method is proposed to evaluate the mixing efficiency of simulation results. The simulation results show that the proposed mixer can achieve full mixing (η >80%) for flow rates up to 15 μL min^{-1} (R_e <2.2) which is acceptable for the typical micromixer working range.

The device was fabricated and the flow was visualized in the channels. A mixing experiment layout was designed by branching the mixer outlet into four branches in order to precisely evaluate the variation of concentration along the outlet cross-section and to assess the mixing performance quantitatively. The acid–base mixing test was performed by measurement of the mixture pH value in each branch. A mixing efficiency of 85% obtained at flow rates less than 40 μL min^{-1} indicates the possibility of obtaining full mixing for R_e <5.5. The results show that the experimental mixing efficiencies are comparable with their corresponding simulation results with a maximum difference of 4.1%. The results established the proposed mixer as a good candidate to be used in real chemical and biological applications that generally operates in low flow rate regime. The whole PDMS structure of the device makes it possible to be easily integrated with other microfluidic devices in a LoC platform for clinical diagnostics and point-of-care applications.

References

1 G. M. Whitesides, *Lab Chip*, 2011, **11**, 191–193.
2 A. J. Demello, *Nature*, 2006, **442**, 394–402.
3 M. Long, M. A. Sprague, A. A. Grimes, B. D. Rich and M. Khine, *Appl. Phys. Lett.*, 2009, **94**, 133501.
4 S. W. Lee, D. S. Kim, S. S. Lee and T. H. Kwon, *J. Micromech. Microeng.*, 2006, **16**, 1067–1072.
5 H. Bockelmann, V. Heuveline and D. P. J. Barz, *Biomicrofluidics*, 2012, **6**, 024123.
6 M. Jain, A. Yeung and K. Nandakumar, *J. Microelectromech. Syst.*, 2009, **18**, 376–384.
7 N. T. Nguyen and X. Huang, *Biomed. Microdevices*, 2006, **8**, 133–139.
8 N. T. Nguyen and Z. Wu, *J. Micromech. Microeng.*, 2005, **15**, R1–R16.
9 C. C. Hong, J. W. Choi and C. H. Ahn, *Lab Chip*, 2004, **4**, 109–113.
10 G. S. Jeong, S. Chung, C. B. Kim and S. H. Lee, *Analyst*, 2010, **135**, 460–473.
11 L. Zhang, H. Nakamura, C. G. Lee and H. Maeda, *RSC Adv.*, 2012, **2**, 3708–3713.
12 E. M. Chan, R. A. Mathies and A. P. Alivisatos, *Nano Lett.*, 2003, **3**, 199–201.
13 H. D. Jin, A. Garrison, T. Tseng, B. K. Paul and C. H. Chang, *Nanotechnology*, 2010, **21**, 445604.
14 P. Watts and S. J. Haswell, *Chem. Soc. Rev.*, 2005, **34**, 235–246.
15 W. Buchegger, A. Haller, S. van den Driesche, M. Kraft, B. Lendl and M. Vellekoop, *Biomicrofluidics*, 2012, **6**, 012803.
16 H. Song and R. F. Ismagilov, *J. Am. Chem. Soc.*, 2003, **125**, 14613–14619.
17 Y. Luo, F. Yu and R. N. Zare, *Lab Chip*, 2008, **8**, 694–700.
18 J. Kim, J. W. Hong, D. P. Kim, J. H. Shin and I. Park, *Lab Chip*, 2012, **12**, 2914–2921.
19 K. P. Nichols, J. R. Ferullo and A. J. Baeumner, *Lab Chip*, 2006, **6**, 242–246.
20 R. T. Tsai and C. Y. Wu, *Biomicrofluidics*, 2011, **5**, 014103.
21 A. A. S. Bhagat, E. T. K. Peterson and I. Papautsky, *J. Micromech. Microeng.*, 2007, **17**, 1017–1024.
22 J. M. Ottino and S. Wiggins, *Science*, 2004, **305**, 485–486.
23 S. H. Wong, P. Bryant, M. Ward and C. Wharton, *Sens. Actuators, B*, 2003, **95**, 414–424.
24 M. X. Lin, K. A. Hyun, H. S. Moon, T. S. Sim, J. G. Lee, J. C. Park, S. Suk Lee and H. I. Jung, *Biosens. Bioelectron.*, 2012, **40**, 63–67.
25 T. Yasui, Y. Omoto, K. Osato, N. Kaji, N. Suzuki, T. Naito, M. Watanabe, Y. Okamoto, M. Tokeshi and E. Shamoto, *Lab Chip*, 2011, **11**, 3356–3360.

26 T. W. Lim, Y. Son, Y. J. Jeong, D. Y. Yang, H. J. Kong, K. S. Lee and D. P. Kim, *Lab Chip*, 2011, **11**, 100–103.
27 T. P. Forbes and J. Kralj, *Lab Chip*, 2012, **12**, 2634–2637.
28 F. Schönfeld, V. Hessel and C. Hofmann, *Lab Chip*, 2004, **4**, 65–69.
29 W. Buchegger, C. Wagner, P. Svasek, B. Lendl, M. Kraft and M. J. Vellekoop, *Sens. Actuators, B*, 2011, **159**, 336–341.
30 C. P. Jen, C. Y. Wu, Y. C. Lin and C. Y. Wu, *Lab Chip*, 2003, **3**, 77–81.
31 K. Ren, W. Dai, J. Zhou, J. Su and H. Wu, *Proc. Natl. Acad. Sci. U. S. A.*, 2011, **108**, 8162–8166.
32 I. H. Shames, *Mechanics of fluids*, McGraw-Hill, New York, 1962.
33 F. Kreith and D. Y. Goswami, *The CRC handbook of mechanical engineering*, CRC Press, 2004.